


Change-point detection in functional time series: Applications to age-specific mortality and fertility

Han Lin Shang* 

Department of Actuarial Studies and Business Analytics
Macquarie University

Abstract

We consider determining change points in a time series of age-specific mortality and fertility curves observed over time. We propose two detection methods for identifying these change points. The first method uses a functional cumulative sum statistic to pinpoint the change point. The second method computes a univariate time series of integrated squared forecast errors after fitting a functional time-series model before applying a change-point detection method to the errors to determine the change point. Using Australian age-specific fertility and mortality data, we apply these methods to locate the change points and identify the optimal training period to achieve improved forecast accuracy.

Keywords: dynamic functional principal component analysis; integrated squared forecast error; long-run covariance function; structural breaks.

1 Introduction

In many developed countries, increases in longevity and an aging population have raised concerns about the sustainability of pensions, healthcare, and aged-care systems (e.g., [Coulmas 2007](#), [Organization for Economic Co-operation and Development \[OECD\] 2013](#)). These concerns have sparked significant interest among government policymakers, planners, demographers, and actuaries in accurately modeling and forecasting age-specific demographic rates.

Many statistical methods have been proposed for forecasting age-specific mortality rates (see reviews by [Currie et al. 2004](#), [Booth 2006](#), [Booth and Tickle 2008](#), [Giroi and King 2008](#), [Shang et al. 2011](#), [Tickle and Booth 2014](#)). Among these, a significant milestone in demographic forecasting is the work of [Lee and Carter \(1992\)](#). They implemented a principal component method to model age-specific mortality rates, extracting a single time-varying index of the level of mortality rates. Forecasts are then obtained from this index using a random walk with drift.

*Postal address: Department of Actuarial Studies and Business Analytics, Level 7, 4 Eastern Road, Macquarie University, Sydney, NSW 2109, Australia; Telephone: +61(2) 9850 4689; Email: hanlin.shang@mq.edu.au.

The Lee-Carter (LC) model is a factor model with age and period effects. In the demographic literature, several extensions have been proposed. From a time-series matrix perspective, [Booth et al. \(2002\)](#), [Renshaw and Haberman \(2003\)](#), [Cairns et al. \(2006\)](#), and [Cairns et al. \(2009\)](#) suggest using more than one component in the LC method to model mortality. [Renshaw and Haberman \(2006\)](#) introduce the age-period-cohort LC method, while [Plat \(2009\)](#) extend the LC model by incorporating age dependencies. Bayesian techniques for LC model estimation and forecasting have been considered by [Giroso and King \(2008\)](#) and [Wiśniowski et al. \(2015\)](#). [Hatzopoulos and Haberman \(2009\)](#) follow a generalized linear model, resulting in models with a structure similar to the LC model but with a generalized error structure. From a time series of functions perspective, [Hyndman and Ullah \(2007\)](#) propose a functional data model utilizing nonparametric smoothing and higher-order principal components. In contrast, [Li and Lee \(2005\)](#), [Hyndman et al. \(2013\)](#), [Shang et al. \(2016\)](#), and [Shang \(2016\)](#) model age-specific mortality for multiple populations jointly. For a comprehensive review of the LC model, refer to the recent survey article by [Basellini et al. \(2023\)](#).

Modeling mortality consists of two parts: (1) estimate a mortality model using historical data; (2) forecasting the time-dependent parameters from the estimated model. The current literature on mortality modeling has primarily focused on creating more extensive mortality models, largely addressing the first part of the process, while the modeling of time-dependent effects in mortality models has not been extensively explored in recent literature, with the exception of [Booth et al. \(2002\)](#). Typically, time-dependent effects (i.e., period and cohort effects) are modeled using autoregressive integrated moving average (ARIMA) models. However, these time-dependent effects may exhibit one or multiple change points. [Booth et al. \(2002\)](#) consider a structural break method applied to the first set of estimated principal component scores. This regression-based method regresses the set of scores against the year. Although the first set of scores explains the most variation in the data, it does not adequately justify the reflection in the scores of a change point in the original data. In the implementation of [Booth et al.'s \(2002\)](#) method, a minimum number of years is set in the fitting period, which is arbitrarily chosen to be 20 years by default. This choice limits the detection of change points.

Various exogenous factors influence mortality over time. Severe short-term events, such as pandemics, wars, and natural disasters, contribute significantly to mortality risks, often resulting in more deaths than expected and introducing spikes in age-specific mortality with lasting effects. In [Booth et al. \(2002\)](#), the observed spike is not due to a crisis but rather a sustained effort to reduce mortality from cardiovascular disease, which included new treatments and lifestyle changes ([Meslé and Vallin 2002](#)). Similarly, government policy interventions aimed at

encouraging childbearing to address low birth rates can have an impact on age-specific fertility rates in many developed countries. Identifying these spikes, known as change points, is crucial in modeling mortality and fertility.

Time series are sequences of measurements over time that describe the behavior of systems. These behaviors can change due to external events and/or systematic internal changes in dynamics distribution. When structural changes are present, standard ARIMA models may not adequately capture time-dependent effects, leading to inconsistent results during the calibration period. [Milidonis et al. \(2011\)](#) propose a regime-switching model with two regimes for different segments of time-varying principal component scores, calibrating the LC model on US data. These two regimes can have different means and variances. [Hainaut \(2012\)](#) extends the regime-switching model to [Renshaw and Haberman's \(2003\)](#) model and finds a significant increase in log-likelihood.

While age is often observed discretely, treating age as a continuous variable may offer advantages. Using interpolation or smoothing, we can obtain $\mathcal{X}_t(u)$ for $t = 1, \dots, n$ where u denotes a continuous variable, such as age. [Hyndman and Shang \(2009\)](#) and [Shang \(2016\)](#) apply functional data analysis to model and forecast age-specific demographic rates for a given year as a continuous function, which can later be discretized into discrete ages at any sampling interval. [Hyndman and Ullah \(2007\)](#) emphasize that the main advantage of functional data analysis is the incorporation of smoothing techniques into the modeling and forecasting of functions, allowing for the natural handling of missing or noisy data. Another advantage is the ability to consider derivatives, a by-product of treating the data as functions (see, e.g., [Shang 2019](#), [Hooker and Shang 2022](#)).

The conditions under which functions are observed over time may undergo changes. There has been increasing interest in detecting and estimating change points in the mean function over time and subsequently estimating locations of change points if they exist. One school of thought is to first reduce the infinite dimension of functional data to a finite dimension via the classic functional principal component analysis, then use the detection method developed for multivariate time series to identify breaks (e.g., [Aue et al. 2009](#), [Berkes et al. 2009](#), [Zhang et al. 2011](#), [Aston and Kirch 2012](#)). The other is a fully functional detection method without preliminary dimension reduction (e.g., [Horváth et al. 2014](#), [Sharipov et al. 2016](#), [Aue et al. 2018](#)), which avoids possible information loss caused by the dimension reduction.

The primary contribution of this paper is to introduce two change point detection methods designed for functional time series and to apply them to age-specific demographic rates. The first method, developed by [Aue et al. \(2018\)](#), utilizes a (scaled) functional cumulative sum

statistic to pinpoint the change point. The second method, developed by [Shang et al. \(2022\)](#), applies a standard structural break method to a time series of integrated squared errors obtained after fitting a functional time-series model. The first method aims to identify the largest gap in the cumulative sum where a change point may occur. The second method transforms the change point detection into a forecasting exercise where a detection method can be applied to the univariate time series of residuals.

The remainder of this paper is organized as follows. Section 2 presents the motivating dataset, which comprises Australian age-specific demographic rates. In Section 3, we introduce two change-point detection methods. Via a series of simulation studies, the comparison of finite-sample performance between the two methods is presented in Section 4. These methods are then applied to identify change points in the Australian age-specific mortality and fertility rates in Section 5. Section 6 concludes with a summary of findings and discusses potential avenues for extending the methodology further.

2 Data sets

2.1 Australian age-specific mortality rates

We analyze Australian age- and sex-specific mortality rates spanning from 1921 to 2020, obtained from the [Human Mortality Database \(2024\)](#). These rates represent the ratio of death counts to population exposure in each respective year and age group (based on one-year intervals). Our study covers age groups from 0 to 99 in single years, with the final group encompassing ages 100 and above. In demographic studies, age-specific mortality rates are often modeled and forecasted using logarithmic transformations for ease of interpretability. To illustrate this, we present rainbow plots for \log_{10} mortality rates (see also [Yang et al. 2022](#)) in Figure 1, where earlier data are depicted in red and more recent data in purple.

Applying the functional KPSS test introduced by [Horváth et al. \(2014\)](#), we obtain p -values of 0.007 and 0.009 for the female and male \log_{10} mortality rates, respectively. Based on these p -values, we conclude that both series exhibit non-stationarity in their mean.

2.2 Australian age-specific fertility rates

Similar to other developed countries, fertility rates in Australia have declined significantly, dropping from 66 per 1,000 in 2007 to 56 per 1,000 in 2020. We examine annual Australian fertility rates spanning from 1921 to 2021 for ages 15–49, sourced from the Australian Bureau

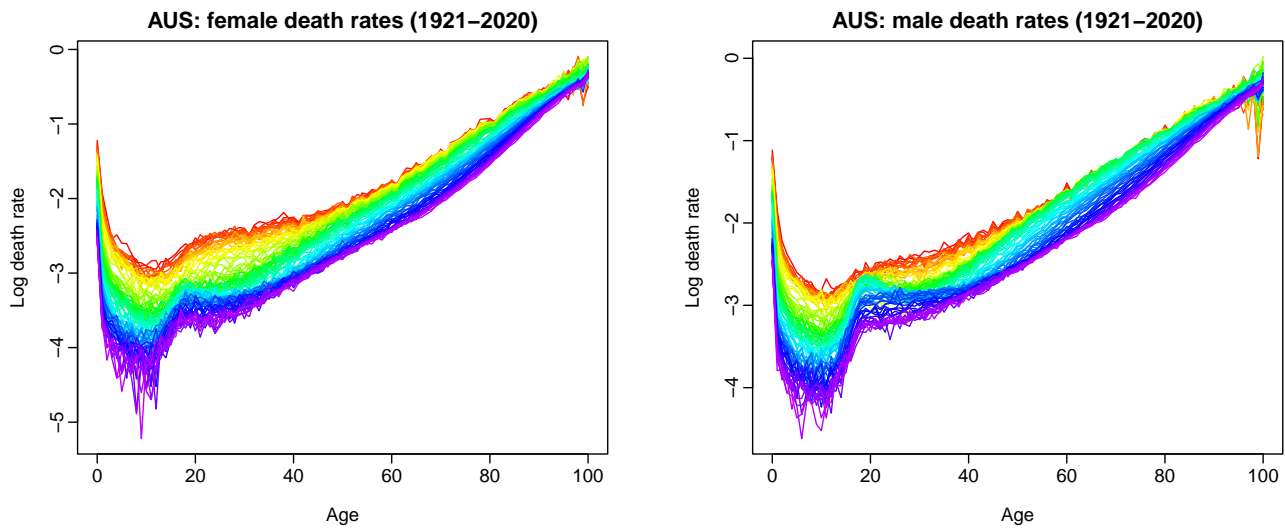


Figure 1: Rainbow plots illustrating Australian age- and sex-specific mortality rates from ages 0 to 100+ between 1921 and 2020.

of Statistics (<https://www.abs.gov.au/statistics/people/population/births-australia/latest-release>). These rates are defined as the number of live births during each calendar year per 1,000 female residents of the same age on 30 June. Figure 2 displays the time series of these age-specific fertility rates.

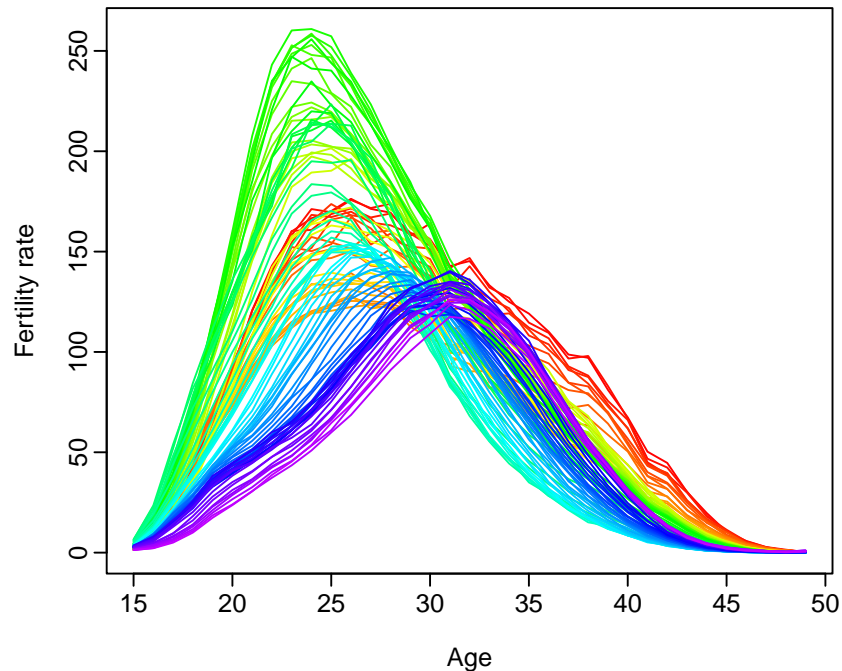


Figure 2: Rainbow plot illustrating Australian age-specific fertility rates between ages 15 and 49 from 1921 to 2021.

Applying the functional KPSS test, we obtain a p -value of 0.045 for the age-specific fertility rates. Based on this result, we conclude that the series is non-stationary in the mean.

3 Change-point detection methods

In the functional time-series literature, there are three types of detection techniques.

- (1) Dimension reduction approach: This method involves reducing the infinite dimensionality of functional data to a finite dimension using functional principal component analysis. Subsequently, detection methods designed for multivariate data are applied to identify breaks (see, e.g., [Aue et al. 2009](#)).
- (2) Fully functional method: To preserve information without dimension reduction, fully functional methods are employed ([Aue et al. 2015](#)).
- (3) Regression-based approach: Another approach involves regression-based methods, such as those discussed by [Shang et al. \(2022\)](#), which are applied to a univariate time series of forecasting errors.

3.1 Fully functional detection method

Denote $[\mathcal{X}_1(u), \mathcal{X}_2(u), \dots, \mathcal{X}_n(u)]$ as a time series of demographic curves, such as age-specific mortality or fertility rates. These observations are generated from a model

$$\mathcal{X}_t(u) = \mu(u) + \delta \mathbb{1}\{t > \eta^*\} + \epsilon_t(u), \quad t = 1, \dots, n,$$

where $\eta^* = \lfloor \vartheta n \rfloor$, with $\vartheta \in (0, 1)$ representing the unknown breakpoint location, $\mathbb{1}\{\cdot\}$ denotes a binary indicator function, and $\mu(u)$ and $\epsilon_t(u)$ denote the mean and error terms, respectively.

[Aue et al. \(2015\)](#) propose a hypothesis test to examine whether $\delta = 0$. The test statistic is constructed based on a scaled functional cumulative sum statistic:

$$S_{n,\eta}^0(u) = \frac{1}{\sqrt{n}} \left(\sum_{t=1}^{\eta} \mathcal{X}_t(u) - \frac{\eta}{n} \sum_{t=1}^n \mathcal{X}_t(u) \right), \quad \eta = 1, 2, \dots, n, \quad (1)$$

where $S_{n,0}^0(u) = S_{n,n}^0(u) = 0$. From (1), we compute the Hilbert-Schmidt norm $\|S_{n,\eta}^0(u)\|$. The test statistic is

$$T_n = \max_{1 \leq \eta \leq n} \|S_{n,\eta}^0(u)\|^2.$$

Under the null hypothesis $H_0 : \delta = 0$,

$$T_n \xrightarrow{D} \sup_{0 \leq x \leq 1} \sum_{\ell=1}^{\infty} \lambda_{\ell} B_{\ell}^2(x), \quad n \rightarrow \infty,$$

where $(B_{\ell} : \ell \in \mathcal{N})$ are independent and identically distributed (i.i.d.) standard Brownian bridges defined on $[0, 1]$, and λ_{ℓ} is the ℓ^{th} eigenvalue of the long-run covariance function specific to functional time series.

To estimate the long-run covariance function, we utilize a kernel sandwich estimator proposed by [Rice and Shang \(2017\)](#). This estimator is designed to capture the long-run covariance, which includes autocovariance up to some finite lag. The long-run covariance is defined as

$$C(u, v) = \sum_{\ell=-\infty}^{\infty} \gamma_{\ell}(u, v)$$

$$\gamma_{\ell}(u, v) = \text{cov}[\mathcal{X}(u), \mathcal{X}(v)],$$


and is a well-defined element of $\mathcal{L}^2(\mathcal{I})^2$, where \mathcal{I} denotes a compact support interval.

In practice, we need to estimate C from a finite sample $\{\mathcal{X}_1(u), \dots, \mathcal{X}_n(u)\}$. Given its definition as a bi-infinite sum, a natural estimator of C is

$$\widehat{C}_{h,q}(u, v) = \sum_{\ell=-\infty}^{\infty} W_q\left(\frac{\ell}{h}\right) \widehat{\gamma}_{\ell}(u, v), \quad (2)$$

where h is called the bandwidth parameter,

$$\widehat{\gamma}_{\ell}(u, v) = \begin{cases} \frac{1}{n} \sum_{j=1}^{n-\ell} [\mathcal{X}_j(u) - \bar{\mathcal{X}}(u)][\mathcal{X}_{j+\ell}(v) - \bar{\mathcal{X}}(v)] & \text{if } \ell \geq 0; \\ \frac{1}{n} \sum_{j=1-\ell}^n [\mathcal{X}_j(u) - \bar{\mathcal{X}}(u)][\mathcal{X}_{j+\ell}(v) - \bar{\mathcal{X}}(v)] & \text{if } \ell < 0. \end{cases}$$

is an estimator of $\gamma_{\ell}(u, v)$ and $W_q(\cdot)$ is a symmetric weight function with bounded support of order q . For the kernel estimator, the critical aspect lies in estimating the bandwidth parameter h . This can be achieved through a data-driven approach, such as the plug-in algorithm proposed in [Rice and Shang \(2017\)](#). Computationally, an  function `long_run_covariance_estimation` is available in the `ftsa` package ([Shang 2013](#), [Hyndman and Shang 2024](#)).

We reject H_0 if T_n exceeds the corresponding quantile of its distribution. The location of the change point is identified with the largest value of $\|S_{n,\eta}^0(u)\|$ for $1 \leq \eta \leq n$. In cases of ties, the change point is identified as the first occurrence.

3.2 Regression-based approach

This method considers a functional change-point detection problem from a forecasting perspective. A standard change-point method can be applied to a univariate time series of forecasting errors. We consider a functional principal component regression, where principal component scores are modeled and forecast by a univariate time-series forecasting method ([Hyndman and Ullah 2007](#)).

Building upon [Martínez-Hernández et al. \(2022\)](#), we extend the functional principal component model from a stationary to a nonstationary functional time series. Nonstationarity is indicated by at least one of the principal component scores $(\widehat{\beta}_{t,1}, \widehat{\beta}_{t,2}, \dots, \widehat{\beta}_{t,K})$ where K is

determined using an eigenvalue ratio criterion. We assume that the nonstationary principal component scores follow an $I(1)$ scalar-valued process. Let $r \in \{1, 2, \dots, K\}$ denote the number of principal component scores that are $I(1)$ processes. While it is possible for $r = K$, it is more common to observe $r < K$, indicating that the remaining $(K - r)$ processes are stationary (see also [Chang et al. 2016](#)). In cases where $r < K$, a portion of the underlying process resides in the nonstationary Hilbert space, while the remainder resides in the stationary Hilbert space. This concept relates to co-integration explored in studies such as [Beare et al. \(2017\)](#), [Seo and Beare \(2019\)](#) and [Seo and Shang \(2024\)](#).

The procedure can be summarized in the following steps.

- 1) Compute the estimated long-run covariance function based on the first-order differenced functional time series, and let $r = \widehat{K}_{\Delta\mathcal{X}}$, where $\widehat{K}_{\Delta\mathcal{X}}$ is the estimated number of functional principal components. We determine r by a modified eigenvalue ratio criterion introduced in [Li et al. \(2020\)](#). The estimated value of r is determined as the integer that minimizes the ratio of two adjacent empirical eigenvalues, given by

$$\widehat{r} = \operatorname{argmin}_{1 \leq k \leq k_{\max}} \left\{ \frac{\widehat{\lambda}_{k+1}}{\widehat{\lambda}_k} \times \mathbb{1}\left(\frac{\widehat{\lambda}_k}{\widehat{\lambda}_1} \geq \theta\right) + \mathbb{1}\left(\frac{\widehat{\lambda}_k}{\widehat{\lambda}_1} < \theta\right) \right\},$$

where k_{\max} is a pre-specified positive integer, θ is a pre-specified small positive number, and $\mathbb{1}(\cdot)$ is the binary indicator function. In the absence of prior information, it is reasonable to choose a relatively large k_{\max} , for example, $k_{\max} = \#\{k | \widehat{\lambda}_k \geq \sum_{k=1}^n \widehat{\lambda}_k / n, k \geq 1\}$ ([Ahn and Horenstein 2013](#)). To prevent over-fitting, we introduce a penalty term for smaller empirical eigenvalues using a threshold constant $\theta = 1 / \ln[\max(\widehat{\lambda}_1, n)]$, ensuring consistency of \widehat{r} .

- 2) With the estimated r , we compute the estimated functional principal components and their associated principal component scores, $\{\widehat{\zeta}_k\}$ and $\{\widehat{\beta}_{t,k}\}$ for $k = 1, 2, \dots, r$. The realizations of the stochastic process \mathcal{X} can be expressed as

$$\mathcal{X}_t(u) = \overline{\mathcal{X}}(u) + \sum_{k=1}^r \widehat{\beta}_{t,k} \widehat{\zeta}_k(u), \quad t = 1, 2, \dots, n,$$

where $\overline{\mathcal{X}}(u) = \frac{1}{n} \sum_{t=1}^n \mathcal{X}_t(u)$.

- 3) Compute the functional residuals: $\mathcal{Z}_t(u) = \mathcal{X}_t(u) - \overline{\mathcal{X}}(u) - \sum_{k=1}^r \widehat{\beta}_{t,k} \widehat{\zeta}_k(u)$.
- 4) Apply [Gabrys and Kokoszka's \(2007\)](#) independence test to the residuals $[\mathcal{Z}_1(u), \dots, \mathcal{Z}_n(u)]$. If the p -value obtained from the independence test is greater than a level of significance $\alpha = 0.05$, then the residuals are deemed independent, and the algorithm terminates. Else, compute the estimated long-run covariance of $[\mathcal{Z}_1(u), \dots, \mathcal{Z}_n(u)]$.

- 5) Apply the eigenvalue ratio criterion to determine the optimal number of retained functional principal components $\widehat{K}_{\mathcal{Z}}$.
- 6) Obtain all estimated functional principal components and their associated principal component scores: $\{\widehat{\zeta}_1(u), \dots, \widehat{\zeta}_r(u), \widehat{\zeta}_{r+1}(u), \dots, \widehat{\zeta}_K(u)\}$ and $\{\widehat{\beta}_{t,1}, \dots, \widehat{\beta}_{t,r}, \widehat{\beta}_{t,r+1}, \dots, \widehat{\beta}_{t,K}\}$ for $t = 1, 2, \dots, n$ and $K = r + \widehat{K}_{\mathcal{Z}}$.
- 7) Obtain forecast scores and forecast curves: using a univariate time-series method, we obtain the principal component score forecast for h -step-ahead, $\widehat{\beta}_{n+h|n,k}$. Multiply these forecast scores by the estimated functional principal components to obtain the forecast curves:

$$\widehat{\mathcal{X}}_{n+h|n}(u) = \overline{\mathcal{X}}(u) + \sum_{k=1}^r \widehat{\beta}_{n+h|n,k} \widehat{\zeta}_k(u) + \sum_{v=r+1}^K \widehat{\beta}_{n+h|n,v} \widehat{\zeta}_v(u).$$

In the forecasting procedure, we begin by generating one-step-ahead point forecasts using the first three functional observations. Subsequently, we expand the sample to include the first four functional observations and re-estimate the parameters within a functional time-series model. We then generate forecasts one step ahead based on the estimated models. This iterative process continues, incrementally increasing the sample size by one observation, until reaching the end of the sampling period. This approach results in 98 one-step-ahead forecasts. To assess point forecast accuracy, we compare these forecasts with the holdout samples (i.e., curves from the 4th to the 101st observations).

To evaluate the accuracy of point forecasts, we employ the integrated squared forecast error (ISFE) (see also [Hyndman and Ullah 2007](#)). This metric quantifies the proximity of forecasts to the actual values of the forecasted variable, and is defined as

$$\kappa_{\gamma+1} = \int_{\mathcal{I}} [\mathcal{X}_{\gamma+1}(u) - \widehat{\mathcal{X}}_{\gamma+1|\gamma}(u)]^2 du, \quad \gamma = 3, \dots, (n-1),$$

where $\mathcal{X}_{\gamma+1}$ represents the $(\gamma+1)$ th holdout sample in the forecasting scheme, and $\widehat{\mathcal{X}}_{\gamma+1|\gamma}(u)$ denotes the one-step-ahead point forecasts for the holdout sample.

Since our objective is to identify the optimal fitting period with one breakpoint (see also [Booth et al. 2002](#)), we estimate the breakpoint using the methodology outlined by [Bai and Perron \(2003\)](#) (see [Zeileis et al. \(2003\)](#) and [Zeileis and Kleiber \(2005\)](#) for detailed implementation descriptions). Suppose we have a time series of integrated squared forecast errors $\kappa_{\gamma+1}$ for $\gamma = 3, \dots, (n-1)$. We estimate a random walk with a piecewise constant drift for the time-dependent variables:

$$\Delta\kappa_{\gamma+1} = \begin{cases} \zeta_1 + \tilde{\zeta}_{\gamma+1} & \gamma + 1 \leq \eta^* \\ \zeta_2 + \tilde{\zeta}_{\gamma+1} & \gamma + 1 > \eta^* \end{cases}$$

where ζ_1 and ζ_2 denote the respective mean terms before and after a breakpoint, and $\tilde{\zeta}_{\gamma+1}$ represents the error term. We estimate this model using ordinary least squares by minimizing the sum of squared residuals (SSR):

$$\text{SSR}(\gamma^*) = \sum_{\gamma=3}^{\gamma^*-1} (\Delta\kappa_{\gamma+1} - \zeta_1)^2 + \sum_{\gamma=\gamma^*}^{n-1} (\Delta\kappa_{\gamma+1} - \zeta_2)^2.$$

This model specification identifies one breakpoint, dividing the univariate time series of forecast errors into two regimes with distinct shifts. The optimal stopping time is selected to minimize the SSR.

4 Simulation studies

We consider three data generating processes previously studied in [Shang et al. \(2022\)](#). The first one considers a stationary functional time series in Section 4.1, where there is an abrupt change occurs at a pre-fixed location. In Sections 4.2 and 4.3, we consider a nonstationary functional time series, where abrupt and gradual changes take place at a randomly assigned location, respectively.

4.1 An abrupt change in the mean of a stationary functional time series

Via a series of Monte-Carlo simulation studies, we evaluate the performance of the two detection methods. The data generating process is a pointwise FAR(1), given by

$$\begin{aligned}\mathcal{X}_1(u) &= 10 \times u \times (1 - u) + \omega \times B_1(u) \\ \mathcal{X}_t(u) &= (\rho + c)\mathcal{X}_{t-1}(u) + \omega \times B_t(u), \quad t = 2, \dots, n \\ \mathcal{Y}_t(u) &= \frac{|\mathcal{X}_{t-1}(u) - \mathcal{X}_t(u)|}{|\mathcal{X}_{t-1}(u) + 0.1|},\end{aligned}$$

where $\{B_t(u), t = 1, \dots, n, u \in [0, 1]\}$ denotes i.i.d. standard Brownian motions. In practice, we discretize continuum u on 101 equally spaced grid points. We consider three values of $\omega = 0.1, 0.5, 0.9$ to reflect three levels of noise to signal. The coefficients satisfy $|\rho| < 1$ and $|\rho + c| < 1$ in order to ensure stationarity. Let $\rho = 0.2$ and $c = 0$ for curves from two to $\tau = \lceil n/2 \rceil$; while $c = 0.7$ for curves from $\lceil n/2 \rceil + 1$ to n .

Table 1: For three sample sizes, we determine the mean, median, standard deviation, and mean squared error of the estimated change points obtained from the two detection methods.

n	τ	ω	$\hat{\tau}$							
			Fully functional				Regression based			
			mean	median	sd	MSE	mean	median	sd	MSE
101	51	0.1	50.27	51	7.70	59.28	51.86	52	17.73	317.61
		0.5	52.39	52	5.87	40.09	50.80	52	18.54	343.91
		0.9	52.45	52	5.76	39.19	50.48	52	18.45	340.12
201	101	0.1	100.60	101	8.76	77.02	100.53	102	30.57	934.08
		0.5	102.53	101	6.84	53.18	98.08	101	32.03	1028.34
		0.9	102.72	101	6.72	52.57	98.19	101	30.73	946.75
401	201	0.1	201.25	201	9.82	97.88	197.98	201	45.36	2059.12
		0.5	203.58	202	8.32	81.89	195.89	201	47.55	2275.74
		0.9	203.59	202	8.12	78.76	194	200	46.38	2185.38

4.2 An abrupt change in the mean of a nonstationary functional time series

We consider another data generating process for simulating functional time series. We begin with simulating a time series of error functions $[\epsilon_1(u), \epsilon_2(u), \dots, \epsilon_n(u)]$ given below:

$$\epsilon_t(u) = \sum_{k=1}^K \beta_{t,k} \phi_k(u) + \varepsilon_t(u),$$

where $[\phi_1(u), \phi_2(u), \dots, \phi_K(u)]$ are randomly sampled with replacement from $K = 21$ Fourier basis functions, and $\varepsilon_t(u)$ denotes an innovation term that can be independent over t . We consider 101 equally spaced grids between 0 and 1.

Let $\beta_t = (\beta_{t,1}, \beta_{t,2}, \dots, \beta_{t,K})^\top$ be a K -dimensional vector. We generate β_t from a vector autoregressive of order 1 (VAR(1)) model,

$$\beta_t = \mathbf{A}\beta_{t-1} + \psi_t, \quad t = 2, \dots, n,$$

where $\mathbf{A} = (a_{ij})_{K \times K}$ is the VAR(1) coefficient matrix, and ψ_t denotes the error terms of the VAR(1) model at time t . Following Li et al. (2020), we consider two structures for coefficient matrix \mathbf{A} .

- (1) \mathbf{A} is a diagonal matrix with diagonal elements drawn from a $U(-0.5, 0.5)$ and ψ_t is generated by a K -dimensional normal distribution with mean zero and power-decay

covariance structure $\text{cor}(\psi_t^i, \psi_t^j) = \rho^{|i-j|}$, where ρ denotes a correlation parameter, such as $\rho = 0.5$.

- (2) Alternatively, \mathbf{A} is a banded autoregressive matrix with $a_{i,j}$ independently drawn from a $U(-0.3, 0.3)$ when $|i - j| \leq 3$ and $a_{ij} = 0$ when $|i - j| > 3$, and ψ_t is independently generated by a K -dimensional normal distribution with mean zero and identity covariance matrix.

To specify a change-point location for the population, we draw a value from a $U(0.25 \times n, 0.75 \times n)$. The lower and upper bounds of the uniform distribution are chosen so that the location of a change point does not lie on the boundary of a sample.

Following [Aue et al. \(2018\)](#), a class of break functions was given by

$$\begin{aligned}\delta_k^*(u) &= \frac{1}{\sqrt{k}} \sum_{w=1}^k \phi_w(u), \quad k = 1, 2, \dots, K, \\ \delta_k(u) &= \delta_k^*(u) \times \sqrt{c},\end{aligned}$$

where the normalization is required to ensure $\delta_k^*(u)$ has unit norm. Here, we consider $\delta_1(u)$ in which the break occurs in the leading eigendirection. The value of c controls the magnitude of the break, and it links to the signal-to-noise (SNR) ratio

$$\text{SNR} = c \times \frac{\mathbf{p} \times (1 - \mathbf{p})}{\text{tr}(\widehat{\mathbf{C}}_\epsilon)},$$

where $\text{tr}(\widehat{\mathbf{C}}_\epsilon)$ denotes the trace of the estimated long-run covariance of the error term. For a given SNR value, we can, in turn, compute the corresponding value of c .

With a chosen eigendirection, such as $k = 1$, we simulate n samples of a non-stationary functional time series as follows:

$$\begin{aligned}\mathcal{X}_t(u) &= \delta_1(u) \times \mathbb{1}\{t > \tau\} + \epsilon_t(u), \\ \mathcal{Y}_t(u) &= \overline{\mathcal{X}}(u) + \mathcal{X}_t(u),\end{aligned}$$

where $\overline{\mathcal{X}}(u) = \frac{1}{n} \sum_{t=1}^n \mathcal{X}_t(u)$.

Table 2 presents some summary statistics of our estimated change points obtained from the two detection methods for three sample sizes for four different SNR ratios. As SNR increases from 0.01 to 0.9, the MSE values decrease, implying that both detection methods make locating the actual change points easier. The fully functional detection method achieves zero MSE values.

Table 2: For three sample sizes, we determine the mean and median of the actual change points, and mean, median, sd, and MSE of the estimated change points under four different signal-to-noise ratios.

n	SNR	True change point τ		Estimated change point $\hat{\tau}$							
		mean	median	Fully functional				Regression based			
				mean	median	sd	MSE	mean	median	sd	MSE
<u>$A = \text{Band}$</u>											
100	0.01	50.07	50	50.07	50	14.20	0	51.21	52	18.87	348.48
	0.1			50.07	50	14.20	0	51.58	52	12.95	5.22
	0.5			50.07	50	14.20	0	51.57	52	12.93	4.52
	0.9			50.07	50	14.20	0	51.57	52	12.93	4.50
200	0.01	99.99	99	99.99	99	29.41	0	99.74	99	40.64	1897.16
	0.1			99.99	99	29.41	0	101.42	100	27.90	13.22
	0.5			99.99	99	29.41	0	101.52	101	28.13	4.61
	0.9			99.99	99	29.41	0	101.52	101	28.13	4.59
400	0.01	200.83	203.50	200.83	203.50	58.36	0	200.01	206	88.73	9403.59
	0.1			200.83	203.50	58.36	0	202.69	206.50	55.93	140.63
	0.5			200.83	203.50	58.36	0	202.28	205.50	57.04	4.64
	0.9			200.83	203.50	58.36	0	202.29	205.00	57.06	4.42
<u>$A = \text{Diag}$</u>											
100	0.01	49.46	49	49.46	49	14.74	0	51.54	52	19.24	353.91
	0.1			49.46	49	14.74	0	51.04	51	13.44	5.94
	0.5			49.46	49	14.74	0	51.02	51	13.45	4.70
	0.9			49.46	49	14.74	0	51.02	51	13.45	4.70
200	0.01	99.6	100	99.6	100	28.54	0	103.05	105	41.35	2007.33
	0.1			99.6	100	28.54	0	101.18	102	26.96	13.21
	0.5			99.6	100	28.54	0	101.11	101	27.25	4.56
	0.9			99.6	100	28.54	0	101.11	101	27.25	4.54
400	0.01	200.39	199.5	200.39	199.5	59.03	0	199.57	205	87.46	9899.3
	0.1			200.39	199.5	59.03	0	201.36	202	57.06	125.59
	0.5			200.39	199.5	59.03	0	201.92	201	57.72	4.98
	0.9			200.39	199.5	59.03	0	201.91	201.5	57.73	4.58

4.3 A gradual change in the mean of a nonstationary functional time series

While Sections 4.1 and 4.2 study stationary and nonstationary functional time series with an abrupt change, in Section 4.2, we alter the data generating process from a sudden change to a gradual change in mean. With the chosen eigendirection $k = 1$, we simulate n samples of a non-stationary functional time series as follows:

$$\begin{aligned}\mathcal{X}_t(u) &= \sqrt{t} \times \frac{n^\alpha}{\sqrt{n}} \times \delta_1(u) \times \mathbb{1}\{t > \tau\} + \epsilon_t(u), \\ \mathcal{Y}_t(u) &= \bar{\mathcal{X}}(u) + \mathcal{X}_t(u),\end{aligned}$$

where t is a time-varying index representing a gradual change. The value of $\alpha \in (0, \frac{1}{2})$ is a constant, along with c controlling the magnitude of the change point. As α or c value increases, the change point size increases; thus it is easier to detect them. In our simulation study, we set $\alpha = 0.5$.

In Table 3, we present some summary statistics of our estimated change points obtained from the two detection methods for three sample sizes for four different SNR ratios. As SNR increases from 0.01 to 0.9, the MSE values decrease, implying that both detection methods make locating the actual change points easier. Note that when SNR=0.5 or 0.9, the regression-based detection method outperforms the fully functional detection methods for $n = 200$ or 400.

Table 3: For three sample sizes, we determine the mean and median of the actual change points, and mean, median, sd, and MSE of the estimated change points under four different signal-to-noise ratios.

n	SNR	True change point τ		Estimated change point $\hat{\tau}$							
		mean	median	Fully functional				Regression based			
				mean	median	sd	MSE	mean	median	sd	MSE
<u>A = Band</u>											
100	0.01	50.07	50	50.79	50	13.19	5.42	52.96	55	19.68	416.13
	0.1			50.63	50	13.36	3.67	51.65	52	12.94	8.17
	0.5			50.63	50	13.36	3.66	51.54	51	12.94	4.42
	0.9			50.62	50	13.37	3.61	51.55	51	12.93	4.45
200	0.01	99.99	99	101.42	99	27.47	21.54	103.46	106	41.38	2041.04
	0.1			101.22	99	27.68	16.95	101.89	101	27.62	33.27
	0.5			101.15	99	27.76	15.24	101.48	101	28.13	4.52

Continued on next page

n	True change point τ				Estimated change point $\hat{\tau}$								
	SNR	mean		median		Fully functional				Regression based			
						mean	median	sd	MSE	mean	median	sd	MSE
	0.9				101.16	99	27.75	15.25	101.50	101	28.13	4.53	
400	0.01	200.83	203.5		203.53	203.5	54.52	74.31	204.53	217	88.91	9622.83	
	0.1				203.30	203.5	54.78	63.44	204.57	209	55.23	302.56	
	0.5				203.25	203.5	54.84	61.75	202.34	205.5	57	5.04	
	0.9				203.23	203.5	54.86	61.11	202.29	204.5	57.06	4.41	
$A = \text{Diag}$													
100	0.01	49.46	49		50.22	49	13.74	5.75	54.05	56	19.67	444.04	
	0.1				50.08	49	13.87	4.07	51.21	51	13.35	9.51	
	0.5				50.08	49	13.87	4.04	51.02	51	13.46	4.68	
	0.9				50.08	49	13.87	3.98	51.02	51	13.45	4.68	
200	0.01	99.6	100		100.82	100	26.84	15.45	103.69	108	42.65	2050.37	
	0.1				100.61	100	27.07	11.94	101.65	102	26.70	28.86	
	0.5				100.60	100	27.09	12.26	101.11	101	27.24	4.62	
	0.9				100.59	100	27.10	12.03	101.10	101	27.25	4.53	
400	0.01	200.39	199.5		202.83	199.5	55.68	64.57	203.48	214.5	88.25	9900.08	
	0.1				202.51	199.5	56.04	52.28	203.07	205	56.97	285.37	
	0.5				202.43	199.5	56.13	48.83	201.97	201	57.68	5.40	
	0.9				202.44	199.5	56.12	48.73	201.90	201	57.73	4.66	

5 Application to age-specific mortality and fertility rates

5.1 Change-point detections

We applied two change-point detection methods to identify the location of the change point. Using the fully functional method, we found change points in 1972 and 1977 for Australian female and male mortality, respectively. The regression-based approach indicated change points in 1976 and 1982. For comparison, implementing the approach by [Booth et al. \(2002\)](#) identified change points in 1981 and 1973.

In the Australian age-specific fertility rates, the fully functional detection method identified

a change point in 1975. Using the regression-based approach, the detected change point was in 1991. For comparison, implementing the approach by Booth et al. (2002) identified a change point in 1974.

5.2 The relationship between the fitting period and forecast accuracy

We investigate how the fitting period influences forecast accuracy by dividing the dataset into training and testing samples. The testing sample comprises the last ten years of data, while the initial training sample includes the remaining data. We employ two change-point detection methods to locate the change point and define the start of the fitting period. Focusing on the LC method, we model and forecast age-specific \log_{10} mortality and fertility rates. The forecasting method remains consistent across experiments, with the sole variation being the length of the fitting period.

For the Australian age-specific fertility rates, we begin with an initial training sample spanning from 1921 to 2011. Using this data, we generate a one-step-ahead forecast for the year 2012. Subsequently, we adopt an expanding window approach, incrementally increasing the training sample by one year and generating one-step-ahead forecasts for each subsequent year up to 2021. This iterative process yields ten one-step-ahead forecasts in total. To evaluate the accuracy of these forecasts, we compare them with the holdout sample from 2012 to 2021.

We assess the point forecast accuracy using the mean absolute percentage error (MAPE), defined as

$$\text{MAPE} = \frac{1}{J \times 10} \sum_{j=1}^J \sum_{\varphi=1}^{10} \frac{|\mathcal{X}_{m+\varphi}(u_j) - \hat{\mathcal{X}}_{m+\varphi|m+\varphi-1}(u_j)|}{\mathcal{X}_{m+\varphi}(u_j)},$$

where $\mathcal{X}_{m+\varphi}(u_j)$ denotes the $(m + \varphi)^{\text{th}}$ holdout curve at a discrete point u_j , and $\hat{\mathcal{X}}_{m+\varphi|m+\varphi-1}(u_j)$ denotes its corresponding forecast.

Using the initial training sample, we apply two change-point detection methods to identify pivotal years. The regression-based approach identifies 1992 as significant, while the fully functional method pinpoints 1974. We then truncate our initial training sample from these identified change points to their respective periods. Subsequently, we employ the LC method to forecast age-specific fertility rates in the testing period.

Figure 3 illustrates comparisons between the holdout sample and forecasts generated from different fitting periods. By juxtaposing the holdout fertility data against these forecasts, we compute the mean absolute percentage error (MAPE) as shown in Table 4.

We divide the Australian age-specific female and male mortality rates into an initial training sample spanning from 1921 to 2010, with a subsequent testing sample covering 2011 to 2020.

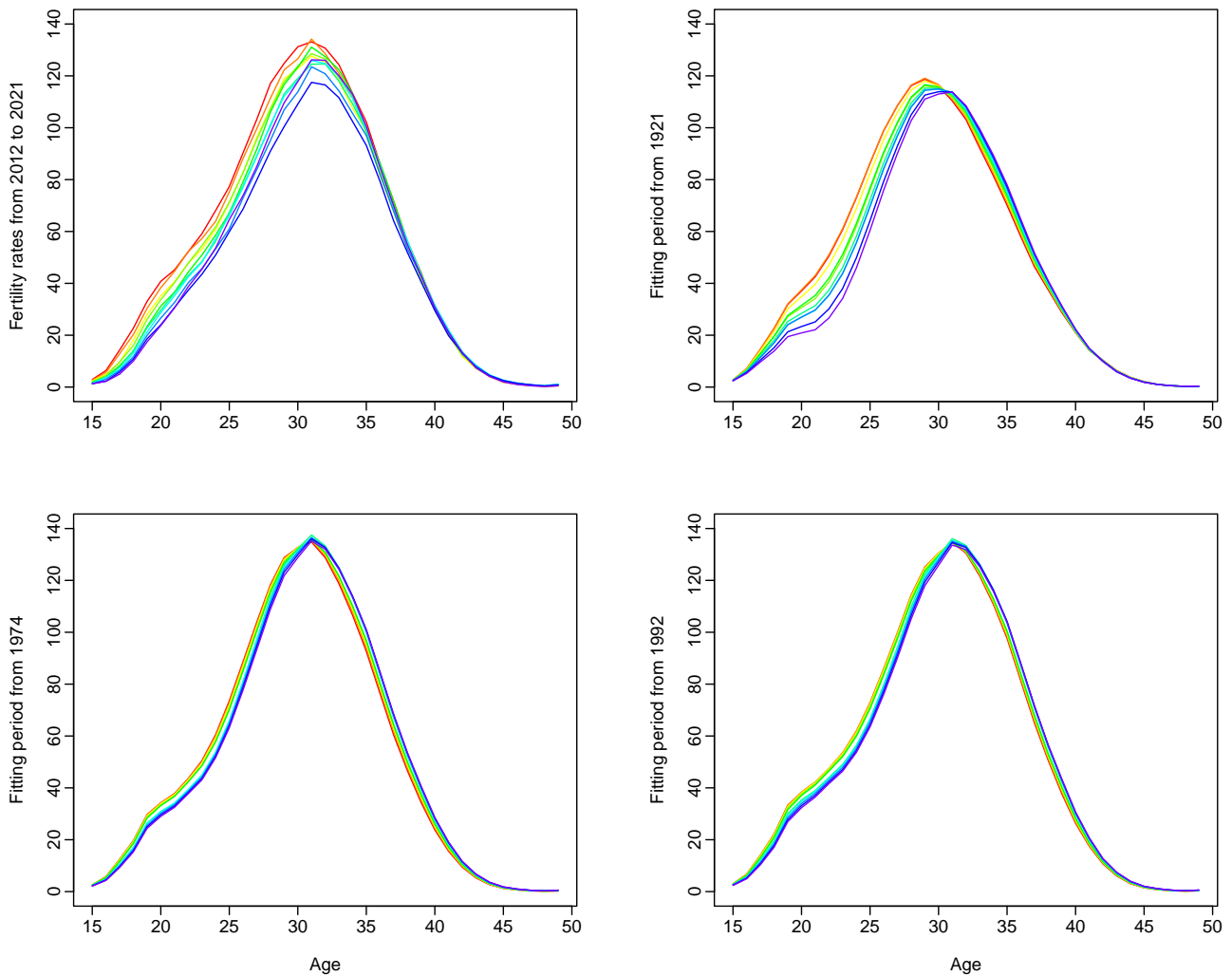


Figure 3: Holdout sample and forecasts of the Australian age-specific fertility rates between 2012 and 2021.


Table 4: A comparison of MAPE between the holdout data and the forecasts. Using the LC method, we consider several change-point detection methods for determining the optimal training sample.

Method	Mortality		Fertility
	Female	Male	
Full sample	3.36	4.16	22.69
Fully functional	1.94	2.27	17.42
Regression-based	1.81	1.96	15.37
Booth et al.'s (2002)	1.88	2.22	17.47

Employing two change-point detection methods, we identify change points in the female series in 1960 (fully functional approach) and 1974 (regression-based approach), while for the male series, change points are identified in 1974 (fully functional approach) and 1982 (regression-based approach). Using the LC method, we generate ten one-step-ahead forecasts of \log_{10}

mortality rates and assess their accuracy using the MAPE.

6 Conclusion

This paper has focused on two change-point detection methods to find breaks in mean functions of functional time series, which exhibit both cross-sectional correlations across ages and temporal dependence. The first method employs a scaled functional cumulative sum statistic to pinpoint the change point, identified as the first location with the highest cumulative sum statistic value. The second method reformulates change-point detection as a forecasting challenge, determining the change point where it yields the largest one-step-ahead forecast errors. Via a series of simulation studies, we evaluate and compare the finite-sample performance of the two detection methods and recommend the fully functional method. Using Australian age-specific mortality and fertility rates data, we successfully identify change points and determine the optimal starting year for the fitting period. By comparing forecasts based on different calibration periods, our findings indicate that reducing the fitting period enhances forecast accuracy. To facilitate reproducibility, the  code is available at https://github.com/hanshang/change_point.

There are several ways in which the methods presented can be extended, and we briefly list four. First, we study several change-point detection methods to locate the change point and find the optimal training sample period. An alternative approach is to adopt the model averaging idea to select the optimal training period implicitly (see, e.g., [Kessy 2022](#), Chapter 3). Second, we demonstrate how the optimal training sample period can affect point forecast accuracy. The presence of a change point can also affect the interval forecast accuracy. Third, we aim to identify a change point for a single functional time series. It is also valuable to explore change-point detection methods for subnational demographic curves, where each series may exhibit a change point. By combining all change points, one can also identify common change points (see, e.g., [Li et al. 2024](#)). Fourth, we choose to locate change points in the age-specific mortality and fertility rates. Alternatively, one can also study the changes in the proportion of causes of death over time (see, e.g., [Nigri et al. 2024](#)).

Conflict of interest

The author declares no competing interests.

Acknowledgements

The author thanks two reviewers, whose valuable comments led to an improved version of this article.

References

- Ahn, S. C. and Horenstein, A. R. (2013), 'Eigenvalue ratio test for the number of factors', *Econometrica* **81**(3), 1203–1227.
- Aston, J. and Kirch, C. (2012), 'Detecting and estimating changes in dependent functional data', *Journal of Multivariate Analysis* **109**, 204–220.
- Aue, A., Gabrys, R., Horváth, L. and Kokoszka, P. (2009), 'Estimation of a change-point in the mean function of functional data', *Journal of Multivariate Analysis* **100**(10), 2254–2269.
- Aue, A., Norinho, D. D. and Hörmann, S. (2015), 'On the prediction of stationary functional time series', *Journal of the American Statistical Association: Theory and Methods* **110**(509), 378–392.
- Aue, A., Rice, G. and Sönmez, O. (2018), 'Detecting and dating structural breaks in functional data without dimension reduction', *Journal of the Royal Statistical Society: Series B* **80**(3), 509–529.
- Bai, J. and Perron, P. (2003), 'Computation and analysis of multiple structural change models', *Journal of Applied Econometrics* **18**(1), 1–22.
- Basellini, U., Camarda, C. G. and Booth, H. (2023), 'Thirty years on: A review of the Lee-Carter method for forecasting mortality', *International Journal of Forecasting* **39**(3), 1033–1049.
- Beare, B. K., Seo, J. and Seo, W.-K. (2017), 'Cointegrated linear processes in Hilbert space', *Journal of Time Series Analysis* **38**(6), 1010–1027.
- Berkes, I., Gabrys, R., Horváth, L. and Kokoszka, P. (2009), 'Detecting changes in the mean of functional observations', *Journal of the Royal Statistical Society: Series B* **71**(5), 927–946.
- Booth, H. (2006), 'Demographic forecasting: 1980 to 2005 in review', *International Journal of Forecasting* **22**(3), 547–581.
- Booth, H., Maindonald, J. and Smith, L. (2002), 'Applying Lee-Carter under conditions of variable mortality decline', *Population Studies* **56**(3), 325–336.

- Booth, H. and Tickle, L. (2008), 'Mortality modelling and forecasting: A review of methods', *Annals of Actuarial Science* **3**(1-2), 3–43.
- Cairns, A. J. G., Blake, D. and Dowd, K. (2006), 'A two-factor model for stochastic mortality with parameter uncertainty: Theory and calibration', *The Journal of Risk and Insurance* **73**(4), 687–718.
- Cairns, A. J. G., Blake, D., Dowd, K., Coughlan, G. D., Epstein, D., Ong, A. and Balevich, I. (2009), 'A quantitative comparison of stochastic mortality models using data from England and Wales and the United States', *North American Actuarial Journal* **13**(1), 1–35.
- Chang, Y., Kim, C. S. and Park, J. (2016), 'Nonstationarity in time series of state densities', *Journal of Econometrics* **192**, 152–167.
- Coulmas, F. (2007), *Population Decline and Ageing in Japan – the Social Consequences*, New York, Routledge.
- Currie, I. D., Durban, M. and Eilers, P. H. C. (2004), 'Smoothing and forecasting mortality rates', *Statistical Modelling* **4**(4), 279–298.
- Gabrys, R. and Kokoszka, P. (2007), 'Portmanteau test of independence for functional observations', *Journal of the American Statistical Association: Theory and Methods* **102**(480), 1338–1348.
- Giroso, F. and King, G. (2008), *Demographic Forecasting*, Princeton University Press, Princeton.
- Hainaut, D. (2012), 'Multidimensional Lee-Carter model with switching mortality processes', *Insurance: Mathematics and Economics* **50**, 236–246.
- Hatzopoulos, P. and Haberman, S. (2009), 'A parameterized approach to modeling and forecasting mortality', *Insurance: Mathematics and Economics* **44**(1), 103–123.
- Hooker, G. and Shang, H. L. (2022), 'Selecting the derivative of a functional covariate in scalar-on-function regression', *Statistics and Computing* **32**(Article number: 35).
- Horváth, L., Kokoszka, P. and Rice, G. (2014), 'Testing stationarity of functional time series', *Journal of Econometrics* **179**(1), 66–82.
- Human Mortality Database (2024), *Max Planck Institute for Demographic Research (Germany), University of California, Berkeley (USA), and French Institute for Demographic Studies (France)*. Available at www.mortality.org (data downloaded on March 16, 2024).
- Hyndman, R. J., Booth, H. and Yasmineen, F. (2013), 'Coherent mortality forecasting: the product-ratio method with functional time series models', *Demography* **50**(1), 261–283.

- Hyndman, R. J. and Shang, H. L. (2009), 'Forecasting functional time series (with discussions)', *Journal of the Korean Statistical Society* **38**(3), 199–211.
- Hyndman, R. J. and Shang, H. L. (2024), *ftsa: Functional time series analysis*. R package version 6.4. URL: <https://CRAN.R-project.org/package=ftsa>.
- Hyndman, R. and Ullah, M. (2007), 'Robust forecasting of mortality and fertility rates: A functional data approach', *Computational Statistics & Data Analysis* **51**(10), 4942–4956.
- Kessy, S. R. (2022), Mortality forecasting with ensembles and combinations, Ph.d. thesis, UNSW Business School.
- Lee, R. D. and Carter, L. R. (1992), 'Modeling and forecasting U.S. mortality', *Journal of the American Statistical Association* **87**(419), 659–671.
- Li, D., Li, R. and Shang, H. L. (2024), 'Detection and estimation of structural breaks in high-dimensional functional time series', *Annals of Statistics* **52**(4), 1716–1740.
- Li, D., Robinson, P. M. and Shang, H. L. (2020), 'Long-range dependent curve time series', *Journal of the American Statistical Association: Theory and Methods* **115**(530), 957–971.
- Li, N. and Lee, R. (2005), 'Coherent mortality forecasts for a group of populations: An extension of the Lee-Carter method', *Demography* **42**(3), 575–594.
- Martínez-Hernández, I., Gonzalo, J. and González-Farías, G. (2022), 'Nonparametric estimation of functional dynamic factor model', *Journal of Nonparametric Statistics* **34**(4), 895–916.
- Meslé, F. and Vallin, J. (2002), 'Mortality in Europe: the divergence between East and West', *Population* **57**(1), 157–197.
- Milidonis, A., Lin, Y. and Cox, S. H. (2011), 'Mortality regimes and pricing', *North American Actuarial Journal* **15**(2), 266–289.
- Nigri, A., Bilancia, M., Cafarelli, B. and Del Gobbo, E. (2024), A methodological framework to monitor changes in proportions of causes of death time series, Working paper, University of Foggia.
- Organization for Economic Co-operation and Development [OECD] (2013), Pensions at a Glance 2013: OECD and G20 Indicators, Technical report, OECD Publishing. Retrieved from http://dx.doi.org/10.1787/pension_glance-2013-en.

- Plat, R. (2009), 'Stochastic portfolio specific mortality and the quantification of mortality basis risk', *Insurance: Mathematics and Economics* **45**(1), 123–132.
- Renshaw, A. E. and Haberman, S. (2003), 'Lee-Carter mortality forecasting: A parallel generalized linear modelling approach for England and Wales mortality projections', *Journal of the Royal Statistical Society: Series C* **52**(1), 119–137.
- Renshaw, A. E. and Haberman, S. (2006), 'A cohort-based extension of the Lee-Carter model for mortality reduction factors', *Insurance: Mathematics and Economics* **38**, 556–570.
- Rice, G. and Shang, H. L. (2017), 'A plug-in bandwidth selection procedure for long run covariance estimation with stationary functional time series', *Journal of Time Series Analysis* **38**(4), 591–609.
- Seo, W.-K. and Beare, B. K. (2019), 'Cointegrated linear processes in Bayes Hilbert space', *Statistics & Probability Letters* **147**, 90–95.
- Seo, W. K. and Shang, H.-L. (2024), 'Fractionally integrated curve time series with cointegration', *Electronic Journal of Statistics* **in press**.
- Shang, H. L. (2013), 'ftsa: An R package for analyzing functional time series', *The R Journal* **5**(1), 64–72.
- Shang, H. L. (2016), 'Mortality and life expectancy forecasting for a group of populations in developed countries: A multilevel functional data method', *The Annals of Applied Statistics* **10**(3), 1639–1672.
- Shang, H. L. (2019), 'Visualizing rate of change: An application to age-specific fertility rates', *Journal of the Royal Statistical Society: Series A* **182**(1), 249–262.
- Shang, H. L., Booth, H. and Hyndman, R. J. (2011), 'Point and interval forecasts of mortality rates and life expectancy: A comparison of ten principal component methods', *Demographic Research* **25**, 173–214.
- Shang, H. L., Cao, J. and Sang, P. (2022), 'Stopping time detection of wood panel compression: A functional time-series approach', *Journal of the Royal Statistical Society: Series B* **71**(5), 1205–1224.
- Shang, H. L., Smith, P. W. F., Bijak, J. and Wiśniowski, A. (2016), 'A multilevel functional data method for forecasting population, with an application to the United Kingdom', *International Journal of Forecasting* **32**(3), 629–649.

- Sharipov, O., Tewes, J. and Wendler, M. (2016), 'Sequential block bootstrap in a Hilbert space with application to change point analysis', *The Canadian Journal of Statistics* **44**, 300–322.
- Tickle, L. and Booth, H. (2014), 'The longevity prospects of Australian seniors: An evaluation of forecast method and outcome', *Asia-Pacific Journal of Risk and Insurance* **8**(2), 259–292.
- Wiśniowski, A., Smith, P. W. F., Bijak, J., Raymer, J. and Forster, J. (2015), 'Bayesian population forecasting: Extending the Lee-Carter method', *Demography* **52**, 1035–1059.
- Yang, Y., Shang, H. L. and Cohen, J. (2022), 'Temporal and spatial Taylor's law: Application to Japanese subnational mortality rates', *Journal of the Royal Statistical Society: Series A* **185**(4), 1979–2006.
- Zeileis, A. and Kleiber, C. (2005), 'Validating multiple structural change models – A case study', *Journal of Applied Econometrics* **20**(5), 685–690.
- Zeileis, A., Kleiber, C., Krämer, W. and Hornik, K. (2003), 'Testing and dating of structural changes in practice', *Computational Statistics and Data Analysis* **44**(12), 109–123.
- Zhang, X., Shao, X., Hayhoe, K. and Wuebbles, D. (2011), 'Testing the structural stability of temporally dependent functional observations and applications to climate projections', *Electronic Journal of Statistics* **5**, 1765–1796.